

## GECAM detection of a bright type-I X-ray burst from 4U 0614+09: confirmation its spin frequency at 413 Hz

Y. P. Chen<sup>1</sup>, J. Li<sup>2,3</sup>, S. L. Xiong<sup>1</sup>, L. Ji<sup>4</sup>, S. Zhang<sup>1</sup>, W. X. Peng<sup>1</sup>, R. Qiao<sup>1</sup>, X. Q. Li<sup>1</sup>, X. Y. Wen<sup>1</sup>, L. M. Song<sup>1</sup>, S. J. Zheng<sup>1</sup>, X. Y. Song<sup>1</sup>, X. Y. Zhao<sup>1</sup>, Y. Huang<sup>1</sup>, F. J. Lu<sup>1</sup>, S. N. Zhang<sup>1</sup>, S. Xiao<sup>1,5</sup>, C. Cai<sup>1,5</sup>, B. X. Zhang<sup>1</sup>, Z. H. An<sup>1</sup>, C. Chen<sup>1,5</sup>, G. Chen<sup>1</sup>, W. Chen<sup>1</sup>, G. Q. Dai<sup>1</sup>, Y. Q. Du<sup>1,8</sup>, M. Gao<sup>1</sup>, K. Gong<sup>1</sup>, D. Y. Guo<sup>1</sup>, Z. W. Guo<sup>1,12</sup>, J. J. He<sup>1</sup>, B. Li<sup>1</sup>, C. Li<sup>1,7</sup>, C. Y. Li<sup>1,6</sup>, G. Li<sup>1</sup>, J. H. Li<sup>1,5</sup>, L. Li<sup>1</sup>, Q. X. Li<sup>1,7</sup>, X. B. Li<sup>1</sup>, Y. G. Li<sup>1</sup>, J. Liang<sup>1,8</sup>, X. H. Liang<sup>1</sup>, J. Y. Liao<sup>1</sup>, J. C. Liu<sup>1</sup>, X. J. Liu<sup>1</sup>, Y. Q. Liu<sup>1</sup>, Q. Luo<sup>1,5</sup>, X. Ma<sup>1</sup>, B. Meng<sup>1</sup>, G. Ou<sup>1</sup>, D. L. Shi<sup>1,8</sup>, F. Shi<sup>1</sup>, J. Y. Shi<sup>1</sup>, G. X. Sun<sup>1</sup>, X. L. Sun<sup>1</sup>, Y. L. Tuo<sup>1</sup>, C. W. Wang<sup>1</sup>, H. Wang<sup>1</sup>, H. Y. Wang<sup>1</sup>, J. Wang<sup>1</sup>, J. Z. Wang<sup>1</sup>, P. Wang<sup>1</sup>, Y. S. Wang<sup>1</sup>, Y. X. Wang<sup>1</sup>, X. Wen<sup>1</sup>, H. Wu<sup>1,8</sup>, S. L. Xie<sup>1,13</sup>, Y. B. Xu<sup>1</sup>, Y. P. Xu<sup>1</sup>, W. C. Xue<sup>1</sup>, S. Yang<sup>1</sup>, M. Yao<sup>1,8</sup>, J. Y. Ye<sup>1</sup>, Q. B. Yi<sup>1,7</sup>, C. M. Zhang<sup>1</sup>, C. Y. Zhang<sup>1,9</sup>, D. L. Zhang<sup>1</sup>, Fan Zhang<sup>1</sup>, Fei Zhang<sup>1</sup>, H. M. Zhang<sup>1</sup>, K. Zhang<sup>1,10</sup>, P. Zhang<sup>1,8</sup>, X. L. Zhang<sup>1,10</sup>, Y. Q. Zhang<sup>1,5</sup>, Z. Zhang<sup>1</sup>, G. Y. Zhao<sup>1,7</sup>, S. Y. Zhao<sup>1,8</sup>, Y. Zhao<sup>1,11</sup>, C. Zheng<sup>1,5</sup>, X. Zhou<sup>1,5</sup>, Y. Zhu<sup>1</sup>

chenyp@ihep.ac.cn,

jianli@ustc.ac.cn, xiongsli@ihep.ac.cn, jilong@mail.sysu.edu.cn

<sup>1</sup> Key Laboratory for Particle Astrophysics, Institute of High Energy Physics, Chinese Academy of Sciences, 19B Yuquan Road, Beijing 100049, China

<sup>2</sup> CAS Key Laboratory for Research in Galaxies and Cosmology, Department of Astronomy, University of Science and Technology of China, Hefei 230026, China

<sup>3</sup> School of Astronomy and Space Science, University of Science and Technology of China, Hefei 230026, China

<sup>4</sup> School of Physics and Astronomy, Sun Yat-Sen University, Zhuhai, 519082, China

<sup>5</sup> University of Chinese Academy of Sciences, Chinese Academy of Sciences, Beijing 100049, China

<sup>6</sup> Physics and Space Science College, China West Normal University, Nanchong 637002,  
China

<sup>7</sup> Key Laboratory of Stellar and Interstellar Physics and Department of Physics, Xiangtan  
University, 411105 Xiangtan, Hunan Province, China

<sup>8</sup> School of Computing and Artificial Intelligence, Southwest Jiaotong University, Chengdu,  
611756, China

<sup>9</sup> Changchun University of Science and Technology, Changchun 130022, Jilin, China

<sup>10</sup> College of Physics and Engineering, Qufu Normal University, Qufu 273165, China

<sup>11</sup> Department of Astronomy, Beijing Normal University, Beijing 100875, China

<sup>12</sup> College of physics Sciences & Technology, Hebei University, Baoding City, Hebei  
Province 071002, China

<sup>13</sup> Institute of Astrophysics, Central China Normal University, Wuhan 430079, China

Received \_\_\_\_\_; accepted \_\_\_\_\_

## ABSTRACT

One month after launching Gravitational wave high-energy Electromagnetic Counterpart All-sky Monitor (GECAM), a bright thermonuclear X-ray burst from 4U 0614+09 was observed on January 24, 2021. We report the time-resolved spectroscopy of the burst and a burst oscillation detection at 413 Hz with a fractional amplitude 3.4% (rms). This coincides with the burst oscillation previously discovered with *Swift*/BAT (Strohmayer et al. 2008), and therefore confirms the spin frequency of this source. This burst is the brightest one in the normal bursts (except the superburst) ever detected from 4U 0614+09, which leads to an upper limit of distance estimation as 3.1 kpc. The folded light curve during the burst oscillation shows a multi-peak structure, which is the first case observed during a single burst oscillation in nonpulsating sources. The multi-peak profile could be due to additional harmonics of the burst oscillation, which is corresponding to several brighter/fainter spots at the stellar surface.

*Subject headings:* stars: coronae — stars: neutron — X-rays: individual (4U 0614+09)  
— X-rays: binaries — X-rays: bursts

## 1. Introduction

Type I X-ray bursts (also known as thermonuclear bursts, “bursts” hereafter) were discovered in the mid-1970s (Grindlay et al. 1976; Belian et al. 1976). They are due to unstable burning of the accreted matter in the atmosphere of neutron stars supplied by the companion star in low-mass X-ray binaries (LMXBs) (for reviews, see Lewin et al. 1993; Cumming 2004; Strohmayer & Bildsten 2006; Galloway et al. 2008). They exhibit spikes in X-ray lightcurves with a fast rise followed by an exponential decay, with a time-scale of 10–100 seconds. Their spectra show a blackbody profile with an evolving temperature of  $kT \sim 1\text{--}3$  keV.

Some strong bursts often exhibit a plateau in the luminosity diagram and an enhancement of the blackbody emission area. It is proposed that the energetic burst emission, i.e., reaching the Eddington limit, temporarily lifts the neutron star photosphere due to radiation pressure. Under this assumption, with a known distance, the mass and radius of neutron star could be inferred.

Nearly 20% bursts show oscillations with fractional amplitudes in the range of 2%–20% rms. The oscillation periods are believed to be around their spin periods although drifting by several Hz in some cases (for reviews, see Watts 2012; Bilous & Watts 2019). Among 115 galactic X-ray bursters, there are only 19 sources in which the detections of burst oscillations are considered robust<sup>1</sup>. Among 11 out of the 19 sources, the pulse signal is absent in the persistent/accretion emission, i.e., they are not accretion-powered millisecond X-ray pulsar. To explain the origin of thermonuclear burst oscillations (TBOs), a brightness asymmetry on the neutron surface is required, which could be driven by different mechanisms, e.g., asymmetries ignition (hotspots) across the neutron stars surface (Strohmayer et al. 1998;

---

<sup>1</sup><https://staff.fnwi.uva.nl/a.l.watts/bosc/bosc.html>

Strohmayer & Markwardt 1999), excitation of large-scale and low-frequency waves (r modes) (Heyl 2004; Chambers et al. 2019) in the neutron star ocean and spreading of a cooling wake to form vortices in the stellar surface (Mahmoodifar & Strohmayer 2016). The former and the latter two models are thought to be related to the TBOs appearance in the rising and decaying phase of the bursts. However, all these mechanisms fail to explain certain aspects of observations, including the absence of TBO during the majority of bursts, up to 48% fractional amplitude of TBOs (Mahmoodifar et al. 2019) and the magnetic field affection on the TBO detection.

The TBO signal of 4U 0614+09 at 415 Hz was first observed with *Swift*/BAT in the tail of a burst (Strohmayer et al. 2008), with a  $4\sigma$  significance assuming a conservative number of trials. However, this TBO was only seen in one time window from one burst, which does not qualify 4U 0614+09 as a robust TBO source (Bilous & Watts 2019).

4U 0614+09 is a faint burster and a persistent LMXB located at the anti-galactic-center direction with a distance of  $\sim 3.2$  kpc and a luminosity mostly dithering  $\sim 1\%$   $L_{\text{Edd}}$  (Kuulkers et al. 2010). Although 4U 0614+09 is one of the closest bursters, only a small number of bursts have been recorded since its discovery in the 1970s. This is due to the long burst recurrence time (on a time scale of weeks) caused by the low accretion rate (Linares et al. 2012). Most of these burst samples were observed by telescopes with a large field of view, e.g., Fermi/GBM and HETE-2/FREGATE.

Thanks to the wide field of view and the high sensitivity to X-ray photons down to about 6 keV, the Gravitational wave high-energy Electromagnetic Counterpart All-sky Monitor (GECAM) (Zhang et al. 2019) detected a burst from 4U 0614+09 during its commissioning phase. We report the spectral and timing results of this thermonuclear burst from 4U 0614+09 in Section 2 and Section 3. In the last Section, the discussion is given.

## 2. Observations and Data analysis

GECAM is a pair of X-ray and gamma-ray all-sky monitors (i.e. GECAM-A and GECAM-B), which aims to search for gamma-ray counterparts to gravitational wave events, which was launched from China Xichang Satellite Launch Center on December 10, 2020 (Beijing time). Two GECAM satellites share the same orbit with an altitude of 600 km and inclination angle of 29 degrees.

Each GECAM satellite has 25 gamma-ray Detectors (GRDs) and 8 charged particle detectors (CPDs). A GRD have a detector diameter 3 inch in diameter, works in 6 keV–5 MeV with a time resolution down to 0.1 us and a energy resolution of 5.3% at 662 keV, which is comprised of LaBr<sub>3</sub>:Ce crystal and the SiPM array.

Each GECAM satellite is designed to cover more than a half sky (i.e. unocculted region by the Earth), thus two satellites in principle could monitor the whole sky. However, there are unexpected power supply issues on satellites, detectors on GECAM-A has not been turned on yet, thus only GECAM-B is used in the rest of this paper.

GECAM-B was triggered in-flight by a long burst at 2021-01-24T11:50:03.600 UTC (MJD 59238.49309722, denoted as  $T_0$ ) (Xiong et al. 2021), which is also used as a reference to extract lightcurve and spectrum. Within the detection location error, 4U 0614+091 lies 2.6° away from the in-flight location. Based on the spectral evolution and in particular the burst oscillation detection as shown below, we confirm that this burst is a genuine thermonuclear X-ray burst from 4U 0614+09 (Chen et al. 2021).

Lightcurves of all the 25 GRDs are extracted and examined one by one according to whether there is a spike around  $T_0$ , among which we find the lightcurvs from detectors #11, #12, #21 and #22 have spikes around  $T_0$ . Therefore, data from these four detectors are used in the following analysis. The lightcurves in 10–25 keV, 10–14 keV, 14-25 keV and the

hardness ratio of the count rates of 10–14 keV to 14–25 keV are shown in Fig. 1. Beyond this energy band, the count rates are dominated by the background emission.

We performed a time-resolved spectroscopy of the burst using a 2 s step. The pre-burst emission was subtracted off as the background during the burst spectral fitting. Response files were generated using `RSP_GENERATOR` from GECAM CALDB v0.3<sup>2</sup>. The time-resolved spectra were fitted using an absorbed blackbody model in the energy range of 10–25 keV, assuming a "TBABS" model (Wilms et al. 2000) and an interstellar hydrogen column density  $N_{\text{H}}$  fixed at  $0.346 \times 10^{-22} \text{ cm}^{-2}$  (Ludlam et al. 2019). The software package XSPEC v12.10.0 was used for the spectral fitting. For the distance in our all calculation, including the luminosity and blackbody radius, we use for a simplicity value of 3 kpc, since the distance is estimated under 15% uncertainty (Kuulkers et al. 2010).

### 3. Results

#### 3.1. Burst spectral evolution

As shown in Fig. 1, the burst has a rise time of 10 s followed by an exponential decay, with a peak flux of 700 cts/s higher than the pre-burst emission in the energy range of 10–25 keV. The hardness diagram indicates a spectral softening during its decay phase. The forementioned profile is common across normal type-I X-ray bursts.

As shown in Fig. 2, the best-fitting parameters are the blackbody temperature  $T_{\text{bb}} \sim 2\text{--}4 \text{ keV}$ , the radius  $R_{\text{bb}} \sim 6 \text{ km}$  with a reduced  $\chi_v \sim 0.7\text{--}1.7$  (16 degrees of freedom). The spectral fitting results and residuals at the burst peak time are shown in Fig. 3. The temperature has a substantial decay along the burst decay phase, which is characteristic to

---

<sup>2</sup><http://gecamweb.ihep.ac.cn/xgwd.jhtml>

thermonuclear bursts. The burst bolometric peak flux is  $\sim 33.0 \pm 1.5 \times 10^{-8}$  erg cm $^{-2}$  s $^{-1}$ , which is corresponding to  $\sim 3.56 \pm 0.2 \times 10^{38}$  erg s $^{-1}$  at a distance of 3.0 kpc. We notice that the peak flux is brighter than the previously report bursts ( $\sim 31.5 \pm 0.5 \times 10^{-8}$  erg cm $^{-2}$  s $^{-1}$ ; Kuulkers et al. 2010) of 4U 0614+91 except for the super-burst, casting some doubt on whether this burst have a PRE phase.

The burst fluence integrating the unabsorbed bolometric luminosities over the whole burst is  $7.5 \pm 0.3 \times 10^{-6}$  erg cm $^{-2}$ , which corresponds to  $8.1 \pm 0.3 \times 10^{39}$  erg assuming a distance of 3 kpc. The burst duration ( $\tau = E_b / F_{pk}$ , ration of the fluence to the peak flux) is  $22.7 \pm 1.4$  s.

The above analysis does not include the gravitational redshift and spectral hardness correction due to the scattering of the photosphere, i.e., the parameters above are apparent values observed from a distant observer. This correction will be given in the discussion part of this work.

### 3.2. Burst oscillation

We considered the burst data within  $T=0-30$  s for timing analysis. Pulsations were searched via an  $Z_n^2$ -test procedure in a narrow frequency range (412–418 Hz) around previously known frequency ( $\sim 415$  Hz, Strohmayer et al. 2008), with a step of 0.003 Hz and a number of harmonics  $n$  varied from 1 to 4. We start from  $Z_1^2$ -test and increase  $n$  until a significant signal is detected. Since no burst activity was observed above 25 keV, only photons in 10–25 keV were included in the timing analysis. We found a peak at  $F = 413.056$  Hz with a  $Z_3^2$  statistic of 35.54 (Figure 4, left panel), which corresponds to a single frequency significance of  $4.65 \sigma$ . To estimate the chance that the timing signal detected above is originated from noise, we calculated the false alarm probability via



implementing a bootstrap method. A simulated event list was constructed. We randomly scattered the same number of observed events in the time range of the burst and carried out the  $Z_3^2$ -test on  $10^4$  simulated event lists and derived the false alarm probability of the detected timing signal, which is  $6 \times 10^{-3}$ . All the sampled frequencies in the  $Z_3^2$ -test have been considered in the bootstrap. Our results are shown in Figure 4, left panel.

We folded the burst events using the best detected frequency (Figure 4, right panel). Based on the folded light curve, the burst oscillation fractional rms amplitude is 3.4%. The phase light curve shows a multi-peak structure, which is different from the sinusoidal profile observed previously in 4U 0614+09 with *Swift*/BAT (Strohmayer et al. 2008). It is quite uncommon and the first time observed among burst oscillations. It may arise from frequency changes/drifts during the type-I burst. To explore this possibility, we searched for timing signals using a sliding window technique, with a data window of 2 s and a sliding step of 0.5 s. We run  $Z_3^2$  timing analysis with a frequency resolution of 0.01 Hz in each data window, and constructed a 2D plane (Figure 4, bottom panel). The timing signal was only significantly detected in a few data windows. The most significant detection is in data window 16–18 s, at  $F = 413.056$  Hz with a  $Z_3^2$  statistic of 30.01 (Figure 4, bottom panel), which corresponds to a single frequency significance of  $4.1 \sigma$ . Simulations were carried out to estimate the false alarm probability, leading to a value of  $2.7 \times 10^{-3}$ . The phase light curve within this data window, or other less significant hot spots in Figure 4, bottom panel, also shows a multi-peak profile. The unique profile of burst oscillation observed in this type-I burst of 4U 0614+09 might be authentic, but could not be further tested because of limited statistics.

#### 4. Discussion

We notice that the observed blackbody radius increases as the flux decrease along with burst cooling, which is not consistent with the emission region corresponding to the whole stellar surface. A possible explanation for this inconformity is related to a spectral hardening factor (color factor) due to electron scattering occurs at the atmosphere outlayer (London et al. 1986). This spectral harden factor ( $f_c \equiv T_\infty/T_{\text{eff}}$ ) depends only on the burst luminosity for a hydrogen-poor composition. It makes the emergent emission deviate from Planck curve, manifesting an overestimation of the temperature by a factor of  $f_c$  and an underestimation of the radius by a factor of  $1/f_c^2$ . For bursts with luminosities brighter than  $0.2 L_{\text{Edd}}$ ,  $f_c$  lies between 1.4 and 1.7, and increases with burst luminosity  $L_{\text{bb}}$ , which causes the anti-correlation between the radius and the flux.

Recent observations found that the stellar atmosphere model also depends on the accretion rate and spectral state of the source. For instance, in atoll sources, the stellar atmosphere model (the spectral hardening factor of bursts) is no longer functional in the high/soft state (the banana state) (Suleimanov et al. 2011; Kajava et al. 2014; Suleimanov et al. 2018). However, in our analysis it is difficult to constrain the accretion-state based on GECAM observation, or *Swift*/BAT and MAXI daily lightcurves, though it appears that 4U 0614+09 spent most of its time in low/hard state (the island state).

We also notice the peak temperature reached up to  $4.0 \pm 0.2$  keV, which is a relatively high value for burst temperature evolution. Given the neutron star mass  $M_{\text{NS}} = 1.4M_\odot$  and radius  $R_{\text{NS}} = 10$  km, a gravitational redshift factor  $(1 + z)$  is estimated as 1.31. Along with  $f_c = 1.7$ , the emergent temperature observed at the stellar surface is revised down to  $T_\infty(1+z)/f_c = 3.0 \pm 0.2$  keV.

Considering the detection of same frequency in two bursts of 4U 0614+09, it qualifies as the 20th source in the sample of robust burst oscillation detection. A dichotomy of burst

oscillations is slow oscillation ( $< 400$  Hz) and rapid oscillation ( $> 400$  Hz) (Galloway et al. 2008; Watts 2012). Mostly, the former group tends to behave short duration ( $\tau < 10$  s), most likely helium-dominated bursts; the latter group tends to behave longer duration ( $\tau > 10$  s) that probably involves mixed hydrogen/helium burning. A possible interpretation is that the slow rotators are largely accreting from degenerate companions with H-deficient composition, and the rapid rotators are non-degenerate companions with more hydrogen composition, but with the exception to this rule: XTE J1814–338, a slow oscillator of 314 Hz but with a long burst duration. Apparently, the burst of this work is a long burst and behaves as a rapid oscillation. Based on the above model, the composition of the burning layer is hydrogen-rich. However, the donor star is proposed to be a degenerate companion, i.e., a C/O-rich donor, which based on the presence of C and O emission lines and absence of H or He emission line on optical spectrum (Nelemans et al. 2004; Werner et al. 2006). Furthermore, the ignition model needs a significant amount of H/He in the accreted material (Cumming & Bildsten 2001; Kuulkers et al. 2010), especially the bursts durations of 4U 1614+91 are several times longer than the well-known pure-He bursts of 4U 1728–34.

The multi-peak profile of the phase lightcurve is the first time reported in a single burst oscillation in nonpulsating sources, although harmonics were reported previously in bursting-pulsars (Chakrabarty et al. 2003; Strohmayer et al. 2003) and 4U 1636–536 by stacking the rising phase of nine bursts (Bhattacharyya & Strohmayer 2005), since additional harmonic is too weak to be detected in a single burst before this work (Chakraborty & Bhattacharyya 2014). A possible reason to cause this profile is that there are more than one antipodal brighter or fainter regions in the NS surface. We notice that phase-folded light curve is beyond the canonical profile (a constant plus a sinusoid) of burst oscillations, which may indicate complicated brightness distribution in the stellar surface. However, the small fractional amplitude of the TBO and the low statistics of the data prevent us to carry out further tests.

Comparing with the other TBOs, we notice that this TBO is a small-amplitude oscillation. In the cooling wake scenario, the behavior of TBO in the burst decay phase is related to the latitude at which the burst ignites, since the first ignition spot being the first cooling spot (Ootes et al. 2017). The ignites latitude could be inferred from the convexity parameter of the lightcurve profile during the burst rising phase, i.e., roughly, a concave and convex profile is responding to high and low ignites latitude (Maurer & Watts 2008). We notice that rising profile of this burst is a convex one, and indicates that it ignites near the equator and induces a short-lived asymmetric emission due to fast speed of the cool wake during the decay phase (Zhang et al. 2016) than the case of the high latitude ignition. This may be related to the small fractional rms of this TBO, since TBO detectability also depends on the time length of the asymmetric emission (Maurer & Watts 2008).

Last but not the least, this burst and the associated oscillation detected by GECAM proves its capability in building a thorough/unique burst sample during GECAM’s service time, thanks to its large detection area and wide field of view: bursts born in the low accretion state or even in the quiescent state of sources can be caught accompanied with the detailed resolution of temporal and spectral properties.

The GECAM (Huairou-1) mission is supported by the Strategic Priority Research Program on Space Science, the Chinese Academy of Sciences, Grant No. XDA15360000. This work is supported by the National Key R&D Program of China (2021YFA0718500), the Key Research Program of Frontier Sciences, Chinese Academy of Sciences, Grant NO. QYZDB-SSW-SLH012 and the National Natural Science Foundation of China under grants 11733009, U1838201, U1838202, U1938101, U2038101, 12173038.

## REFERENCES

- Bhattacharyya, S., & Strohmayer, T. E. 2005, *ApJL*, 634, L157
- Bilous, A. L. & Watts, A. L. 2019, *ApJS*, 245, 19
- Belian, R. D., Conner, J. P., & Evans, W. D. 1976, *ApJ*, 206, L135
- Brandt, S., Castro-Tirado A. J., Lund, N., et al. 1992, *A&A*, 262, L15
- Chakraborty, M., & Bhattacharyya, S. 2014, *ApJ*, 792, 4
- Chakrabarty, D., Morgan, E. H., Munro, M. P., et al. 2003, *Nature*, 424, 42
- Chambers, F. R. N., Watts, A. L., Keek, L., Cavecchi, Y., & Garcia, F. 2019, *ApJ*, 871, 61
- Chen, Y. P., Li, J. Xiong, S. L. et al. 2021, *ATEL*, 14363
- Cumming, A., & Bildsten, L. 2001, *ApJ*, 559, L127
- Cumming, A. 2004, *Nucl. Phys. B Proc. Suppl.*, 132, 435
- Galloway, D. K., Munro, M. P., Hartman, J. M., et al. 2008, *ApJS*, 179, 360
- Grindlay, J., Gursky, H., Schnopper, H., et al. 1976, *ApJ*, 205, L127
- Heyl, J. S. 2004, *ApJ*, 600, 939
- Kajava, J. J. E., Nättilä, J., Latvala, O. M., et al. 2014, *MNRAS*, 445, 4218
- Kuulkers, E., in't Zand, J. J. M., Atteia, J. L. et al. *A&A* 514, A65
- Lewin W. H. G. et al. 1976, *ApJ*, 207, L95
- Lewin, W. H. G., van Paradijs, J., & Taam, R. E. 1993, *Space Sci. Rev.*, 62, 223
- Linares, M., Connaughton, V., Jenke, P. et al. 2012, *ApJ*, 760, 133

- London, R. A., Taam, R. E., Howard, W. M. 1986, ApJ, 306, 170
- Ludlam, R. M., Miller<sup>1</sup>, J. M., Barret, D. et al. 2019, ApJ, 873,99
- Mahmoodifar, S., & Strohmayer, T. E. 2016, ApJ, 818, 93
- Mahmoodifar, S., Strohmayer, T. E., Bult, P. et al. 2019, ApJ, 878, 145
- Maurer, I., & Watts, A. L. 2008, MNRAS, 383, 387
- Nelemans, G., Jonker, P. G., Marsh, T. R., van der Klis, M. 2004, MNRAS, 348, L7
- Ootes, L. S., Watts, A. L., Galloway, D. K., & Wijnands, R. 2017, ApJ, 834, 21
- Strohmayer, T. E., & Bildsten, L. 2006, New views of thermonuclear bursts (Compact stellar X-ray sources), 113, 156
- Strohmayer, T. E., Markwardt, C. B., & Kuulkers, E. 2008, ApJL, 672, L37
- Strohmayer, T. E., Zhang, W., Swank, J. H. et al. 1998, ApJ, 498, 135
- Strohmayer, T. E. & Markwardt, C. B. 1999, ApJ, 516, 81
- Strohmayer, T. E., Markwardt C. B., Swank J. H., in't Zand J. J. M., 2003, ApJ, 596, L67
- Suleimanov, V. F., Poutanen, J., Revnivtsev, M., & Werner, K. 2011, ApJ, 742, 122
- Suleimanov, V. F., Poutanen, J., Werner, K. 2018, A&A, 619, 114
- Watts, A. L. 2012, ARA&A, 50, 609
- Werner, K., Nagel, T., Rauch, T. et al. 2006, A&A, 450, 725
- Wilms, J., Allen, A., McCray, R. 2000, ApJ, 542, 914
- Xiong, S. L., Lu, F. J., Zhang, S. N. et al. 2021, GCN, 29450

Zhang, D. L., Li, X. Q., Xiong, S. L. et al. 2019, Nuclear Instruments and Methods in Physics Research Section A, 921, 8

Zhang, G. B., Méndez, M., Zamfir, M., & Cumming, A. 2016, MNRAS, 455, 2004

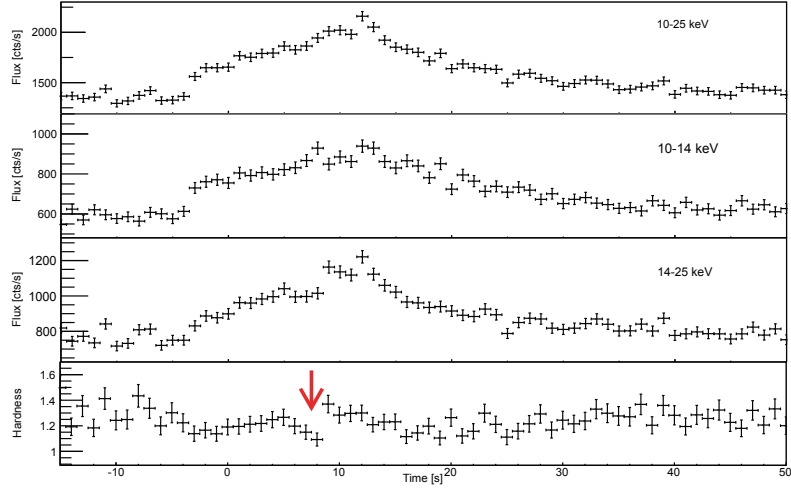


Fig. 1.— The burst light curves in 10–25 keV, 10–14 keV, 14–25 keV and the harness ratio of the flux in 14–25 keV to 10–14 keV. The red arrow in the bottom panel marks the dip in the hardness, which indicates a possible PRE during the burst.



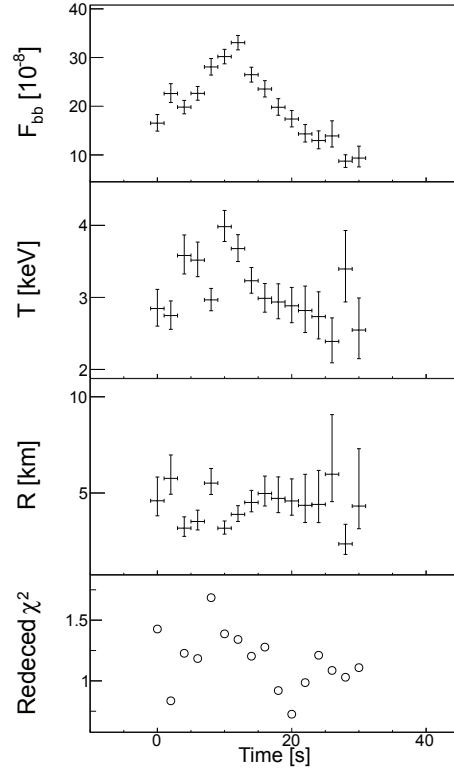


Fig. 2.— Time-resolved spectroscopy of the X-ray burst using an absorbed blackbody model, with a time step 2 s. The unabsorbed bolometric flux  $F_{\text{bb}}$  in a unit of  $10^{-8} \text{ erg cm}^{-2} \text{ s}^{-1}$  (top panel), the temperature  $kT$  (2nd panel), the radius  $R$  at a distance of 3 kpc (3rd panel) and the reduced  $\chi^2$  statistic (bottom bottom) are given in the 4 panels, respectively.

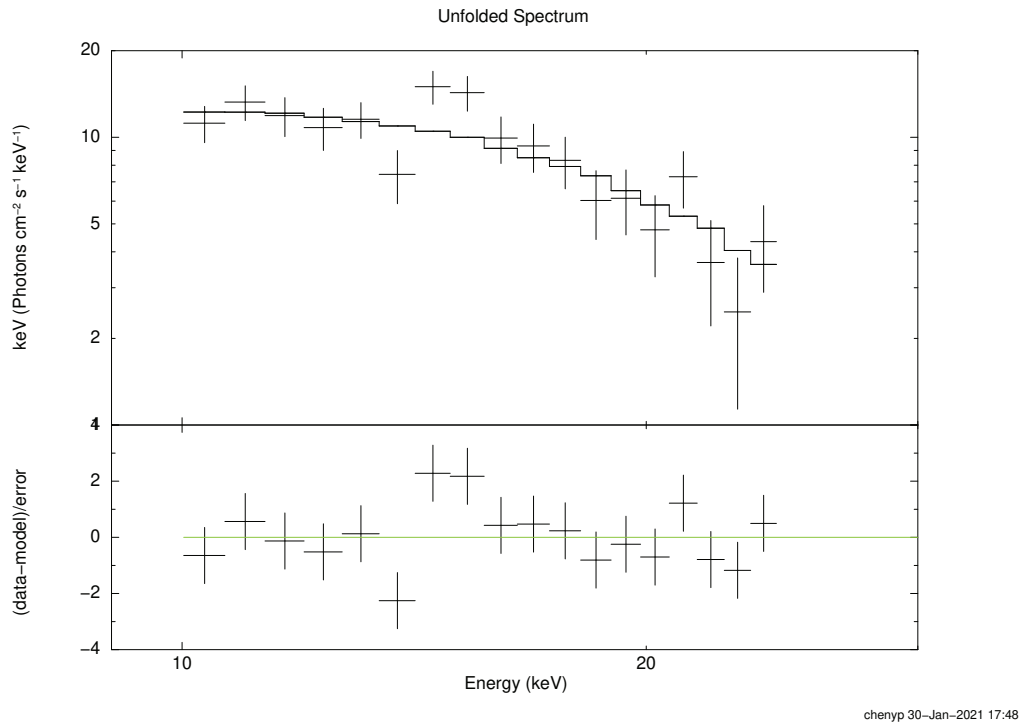


Fig. 3.— The spectra of the burst peak emission fitting by a blackbody model.

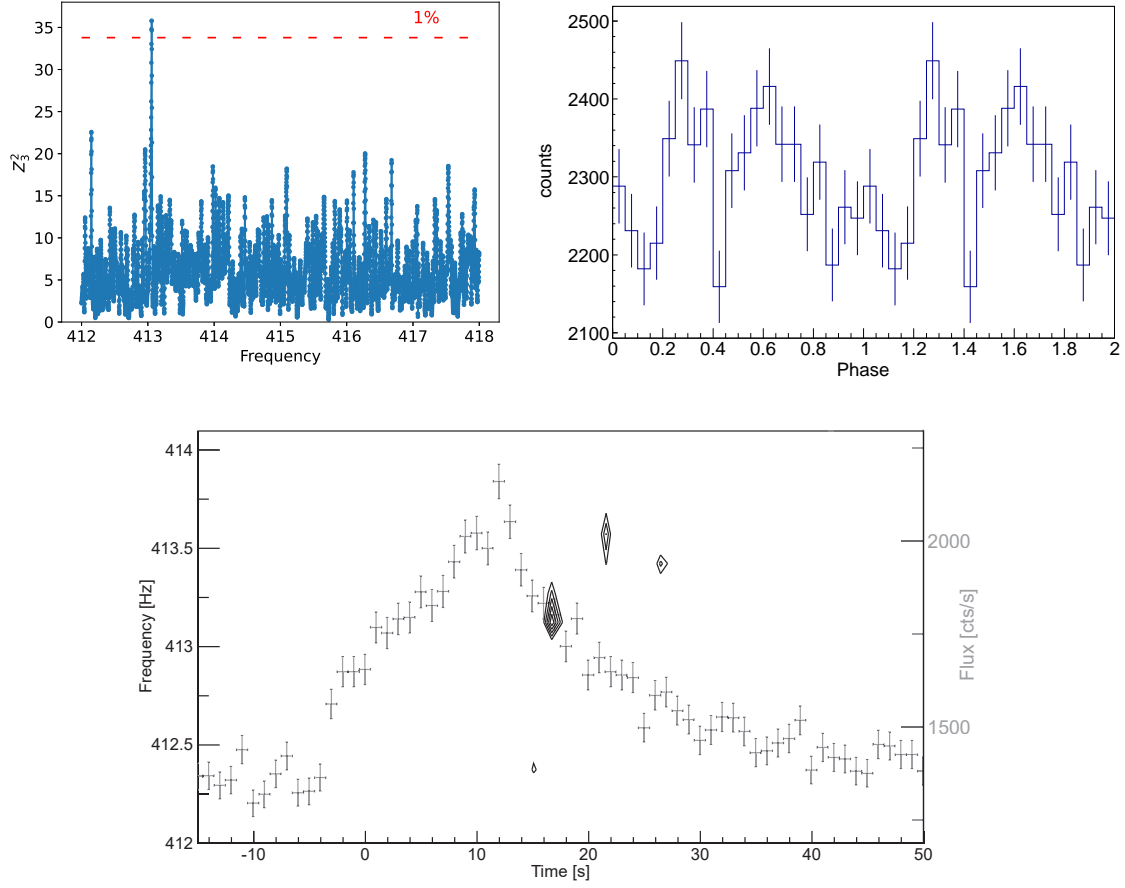


Fig. 4.— Left:  $Z_3^2$  periodogram of 4U 0614+09 during the type-I burst. The red dashed line indicates false alarm probability of 1% level. Right: Phase light curve of 4U 0614+09 with the best detected frequency. Bottom: The Power spectra using 2 s intervals and stepped the intervals by 0.5 s, five contour levels of the  $Z_3^2$  are plotted, starting at 15 and spaced in steps of 2.

